Photonic generation of triangular and rectangular waveforms based on four-wave mixing effect*

YUAN Jin, WANG Yujie, ZHANG Hui, ZHANG Mengsi, and LI Zengrui**

State Key Laboratory of Media Convergence and Communication, Communication University of China, Beijing 100044, China

(Received 27 June 2021; Revised 27 September 2021)

A photonic approach that can generate triangular and rectangular waveforms is proposed. A dual-electrode Mach-Zehnder modulator (De-MZM) is used to fulfill the external optical carrier suppression (OCS) modulation of a continuous wave (CW). The follow-up four-wave mixing (FWM) in a semiconductor optical amplifier (SOA) makes four primary sidebands exist in the spectrum. Then filtering and optical carrier recovery techniques are used to construct the spectrum aligning with that of a triangular/rectangular waveform. In this work, we also elaborate the influence of errors of key device parameters, by which the feasibility and stability of the system have been verified. Based on this photonic approach, a 10 GHz full-duty-cycle triangular waveform and a 50%-duty-cycle rectangular waveform are successfully obtained. This approach provides a feasible method to generate multiple waveforms.

Document code: A **Article ID:** 1673-1905(2022)01-0006-7

DOI https://doi.org/10.1007/s11801-022-1102-1

Photonic arbitrary waveforms have been extensively used in high-speed all-optical network systems because of their advantages such as large bandwidth, low loss, powerful anti-electromagnetic interference (EMI), and superior flexibility. Numerous studies have also shown that the microwave photonics can effectively replace the electronic methods suffering from small bandwidth, low center frequency and large timing jitter, and has been proved to be a promising technical means[1-3]. Among varieties of arbitrary waveforms, triangular and rectangular waveforms are widely applied in pulse compression technology, signal regeneration or copying, all-optical communication systems and so on. Hence, it is an important issue to study the generation of triangular and rectangular waveforms.

Using the frequency-to-time mapping (FTTM)[4,5] to generate arbitrary waveforms is one of the current popular methods. For proposals in Ref.[4], an amplified spontaneous emission (ASE) enters into a special fiber grating to alter the pulse spectrum, and then is combined with a dispersive fiber to realize the FTTM. However, this method cannot guarantee the accuracy and flexibility of the generated signal. Moreover, the duty cycle of the obtained waveforms is generally less than 1. In recent years, the waveform generation using an optoelectronic oscillator (OEO) has also become a hot research topic[6,7]. In a waveform generator system based on an OEO, an independent radio frequency signal is no longer needed to drive the modulator. For example, a scheme based on cascaded modulators and an OEO was proposed in Ref.[6]. MA et al[7] proposed square, sawtooth (reversed-sawtooth) and triangular waveform generator based on a dual-loop OEO structure. These configurations mentioned above are generally at the expense of system complexity to realize the microwave waveforms generation. Proposal based on external modulation method provides new idea for simplifying the complexity of the system. The most well-known methods are the time domain synthesis (TDS)[8,9] and the frequency domain synthesis (FDS)[10-14]. ZHANG et al[8] put forward the use of a dual-polarization modulator to synthesize the triangular, flat top and sawtooth pulse trains in time domain. In Ref.[9], a continuous wave (CW) is firstly transmitted to cascaded single-drive Mach-Zehnder modulators (SD-MZMs) biasing at quadrature points, and then using the engraving and overlapping of time-domain waveforms to obtain the target arbitrary waveforms. Currently, FDS based on the external modulation method for generating waveforms is prevalent. A series of photonic microwave waveform generation methods based on FDS is proposed[10-13]. For example, in Ref.[10], the Sagnac loop is utilized to generate the optical signals of ±1st-order and ±3rd-order sidebands. Thanks to the stimulated Brillouin scattering (SBS) effect, the microwave signal consisting of odd order harmonics is generated after the photodetector (PD), which can construct the triangular waveform, the square waveform, or the sawtooth waveform by adjusting the weight

* This work has been supported by the National Natural Science Foundation of China (No.62105306).
** E-mail: yuanjin@cuc.edu.cn

of the harmonics. In Ref.[12], a triangular shaped microwave pulse is generated by optical heterodyning principle using SBS. However, the gain requirements of the SBS are very strict, and precise frequency shifting isrequired to amplify or attenuate the power of the optical carrier. In Ref.[13], a scheme based on a dual-electrode MZM (De-MZM) and a normal dispersion fiber (NDF) to generate a photon triangular pulse is presented. The difficulty of this scheme is the requirement of an accurate dispersion value.

In this paper, we put forward a triangular/rectangular waveform generator, using external modulation in a De-MZM and four-wave mixing (FWM) in a semiconductor optical amplifier (SOA). A CW in the upper-branch is firstly executed optical carrier suppression (OCS) modulation by a De-MZM. Subsequently, the modulated signal enters an SOA for non-linear modulation, so that the anti-interference ability of the generated signal is enhanced. The CW in the lower-branch is used to recover the suppressed optical carrier. An optical band pass filter (OBPF) is applied to filter out the negative sidebands. We elaborate the influence of the bias current of an SOA, the modulation index and the extinct ratio of the De-MZM, as well as the imbalance ratio of the 180° hybrid couple on the generated waveforms. In our simulation, by properly adjusting parameters, the triangular and rectangular waveforms with repetition rates of 10 GHz are achieved.

Schematic diagram in Fig.1 is the proposed generator structure of triangular and rectangular waveforms.

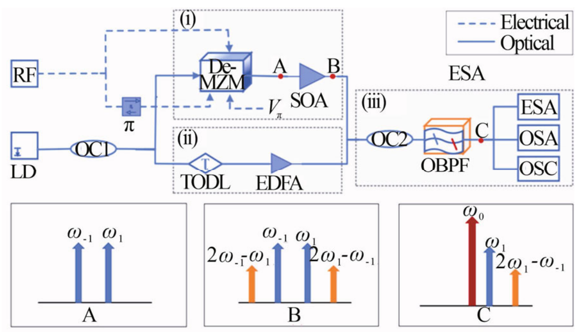

Fig.1 Schematic of the proposed photonic triangular and rectangular waveforms generator

The optical field distribution of the CW source light can be expressed as $E_{in}(t)=E_0\exp(j\omega_0 t)$, where E_0 is the amplitude of the optical field, and ω_0 denotes the angular frequency. And then the CW is divided into upper and lower branches by OC1. As in Configuration (i) in the upper-branch, a radio frequency (RF) signal $V_{RF}(t)=\sqrt{2}V_{RF}\sin\omega_{RF}t$ splitted into two parts with a 180° difference to drive the two electrodes of the De-MZM. When De-MZM is biased at the minimum transmission point (MITP), the modulator is working at OCS modulation. The optical field mathematical expression of signal at point A is[23]

$$E_A(t)=\frac{E_{in}(t)}{t_{ff}}\{\gamma\cdot\exp(jm\sin\omega_{RF})+$$
$$(1-\gamma)\cdot\exp(-jm\sin\omega_{RF}t+j\varphi)\},\tag{1}$$

where t_{ff} and ε_r are the insertion loss and the extinction ratio of the De-MZM, respectively. $\gamma=1/2(1+1/\sqrt{\varepsilon_r})$ is a relation expression of the power distribution ratio at the input and output of the Y-branch waveguide. $m=\pi V_{RF}/V_\pi$ is the modulation index, $\varphi=\pi V_{bias}/V_\pi$ is the bias-induced phase shift. Assuming that t_{ff}=1/2, $\varepsilon_r=\infty$, γ can be calculated as 1/2. Expanding Eq.(1) with Jacobi-Auger expansion, the optical field can be rewritten as

$$E_A(t)=\frac{1}{2}E_{in}(t)\{\sum_{n=-\infty}^{\infty}J_n(m)\exp(jn\omega_{RF}t)+$$
$$\sum_{n=-\infty}^{\infty}(-1)^n J_n(m)\exp(jn\omega_{RF}t+j\varphi)\},\tag{2}$$

where J_n denotes Bessel function of the nth-order of the first kind. The relation between the modulation index m and the Bessel function $J_n(m)$ is given in Fig.2.

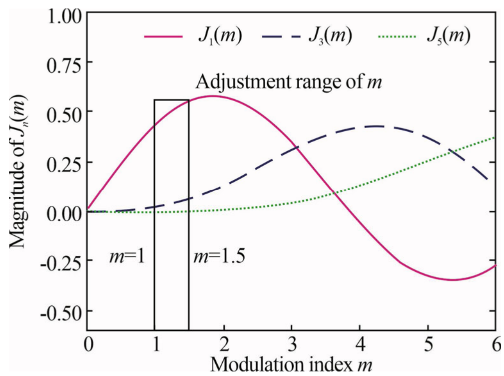

Fig.2 $J_{2n-1}(m)$ versus modulation index m

From this graph, it can be clearly seen that when m is in the range of $1\leq m\leq 1.5$, the 1st-order harmonic component $J_1(m)$ is much higher than $J_3(m)$ and $J_5(m)$. Therefore, harmonic components higher than 1st-order can be ignored. After OCS modulation, only ±1st-order sidebands are retained as shown in the Fig.1(a). The optical field distribution at point A can be abbreviated as

$$E_A(t)\propto\left[\exp\left(j\omega_1 t\right)+\exp\left(j\omega_{-1}t\right)\right].\tag{3}$$

The ±1st-order optical sidebands are injected to an SOA to act as the pump light of FWM effect[14]. The FWM in an SOA is an optical nonlinear effect caused by the third-order nonlinear polarization of the medium. The FWM effect is an ultra-fast nonlinear process, and it can well maintain amplitude and phase information of the original signal. Here, degenerate four-wave mixing is used[15]. The wave number corresponding to the light wave frequency ω_p can be expressed as $K_p=n_p\omega_p/c$, where n_p is the effective refractive index corresponding to different modes. The phase matching condition under different light wave frequencies is $\Delta K_{mlj}=2K_m-K_l-K_j$. To excite four-wave mixing to obtain two idle frequency lights, the input pump light and signal light need to meet the phase matching condition ΔK=0. After FWM in SOA, there are four optical sidebands in the spectrum as shown in Fig.1(b). Supposing that the amplitudes of the ±1st-order sidebands are α and β, the amplitudes of the newly generated sidebands are α_1 and β_1, respectively. Use output sideband to express the optical field distribution as

$$E_B(t) = \{\alpha_1 \cdot \exp\left[j\left(2\omega_1 - 2\omega_{-1}\right)t\right] + \alpha \cdot \exp\left(j\omega_{-1}t\right) + \beta \cdot \exp\left(j\omega_1 t\right) + \beta_1 \cdot \exp\left[j\left(2\omega_{-1} - 2\omega_1\right)t\right]\}. \quad (4)$$

Then in the Configuration (ii), a tunable optical delay line (TODL) is inserted to ensure the correlation between the upper- and lower-branch of the optical signals. The CW light in the lower-branch is fed into an EDFA to obtain an amplified optical carrier signal with a power higher than 1st-order harmonic component. For Configuration (iii), two branches optical signals are coupled into an OC. As the weights of frequency components after FWM are not completely symmetrical, we use an OBPF to filter out the negative sidebands and only use the positive sidebands to construct the target waveform, as shown in Fig.1(c). By substituting $\omega_1=\omega_0+\omega_{RF}$, $\omega_1=\omega_0-\omega_{RF}$ into Eq.(4), the optical field distribution at point C can be expressed as

$$E_C(t) = \{\mu \cdot \exp\left(j\omega_0 t\right) + \beta \cdot \exp\left[j\left(\omega_0 + \omega_{RF}\right)t\right] + \beta_1 \cdot \exp\left[j\left(\omega_0 + 3\omega_{RF}\right)t\right]\}, \quad (5)$$

where μ represents the amplitude of the recovered optical carrier. The corresponding optical field intensity at point C is

$$I_C(t) \propto \{\left(\beta^2 + \beta_1^2 + \mu^2\right) + 2\beta\mu \cdot \cos\left(\omega_{RF}t\right) + 2\beta\beta_1 \cdot \cos\left(4\omega_{RF}t\right) + 2\beta_1\mu \cdot \cos\left(3\omega_{RF}t\right)\}. \quad (6)$$

To ensure the generation of the triangular and rectangular waveforms, it is necessary to guarantee that the power difference between the amplified optical carrier and the 1st-order harmonic is large enough. This means that for a big value of μ, $\beta\beta_1$ is much smaller than $\beta\mu$ and $\beta_1\mu$. In this case, only items of DC component, $\cos(\omega_{RF}t)$ and $\cos(3\omega_{RF}t)$ are retained in Eq.(6). The intensity distribution of the final output signal can be simplified as

$$I_C(t) \propto \left\{I_{DC} + \cos\left(\omega_{RF}t\right) + \frac{\beta_1}{\beta}\cos\left(3\omega_{RF}t\right)\right\}. \quad (7)$$

The Fourier expansion of the ideal triangular waveform is

$$T_{tr}(t) \propto \cos(\omega t) + \frac{1}{9}\cos(3\omega t) + \frac{1}{25}\cos(5\omega t) + \ldots. \quad (8)$$

By comparing Eq.(8) with Eq.(7), it can be drawn that the generation of a triangular waveform needs to satisfy the condition of β_1/β=1/9. In other words, the amplitude ratio of the +1st-order and the newly generated sidebands should be 9. Power difference is used to describe this relationship in spectrum, P_Ω/P_{new}=10lg(β_1^2/β^2)≈19 dB. In the following work, we need properly set parameters of SOA bias current G and modulation index m to satisfy P_Ω/P_{new}≈19 dB. As stated in Fig.2, the required m is in the range from 1 to 1.5. Result in Fig.3(a) shows the variation of P_Ω/P_{new} with the change of bias current G when m is fixed as 1.43. It proves that when G is 0.146 5 A, the value of P_Ω/P_{new} is desired 19 dB. In turn, taking G as 0.146 5 A, Fig.3(b) depicts the relationship between P_Ω/P_{new} and m. As m varies from 1 to 1.5, the value of P_Ω/P_{new} jitters in the proximity of 19 dB and the oscillation is smaller than 0.7 dB. It fully shows that a wide range of m can be selected to ensure P_Ω/P_{new}≈19 dB.

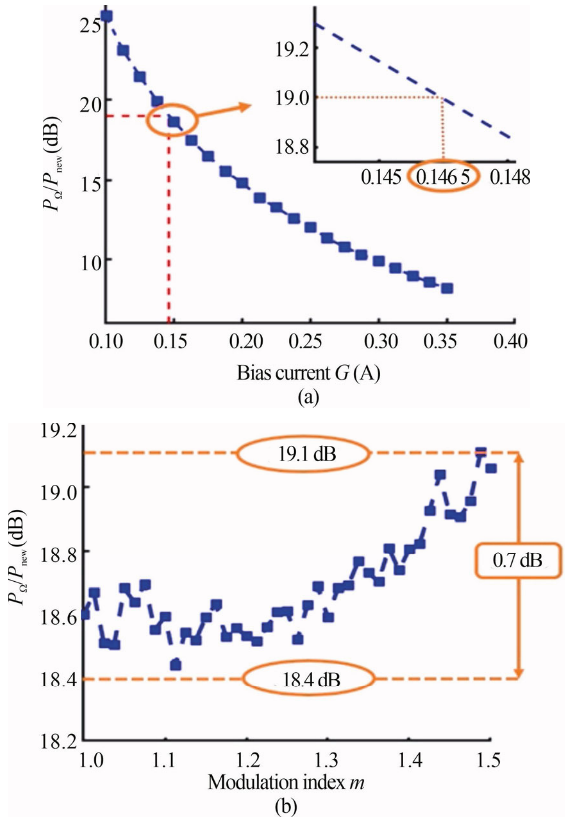

Fig.3 (a) The relevance of P_Ω/P_{new} and the bias current G when m is set as 1.43; (b) The relevance of P_Ω/P_{new} and modulation index m when G is 0.146 5 A

In the above theoretical analysis, it is assumed that the extinction ratio of the De-MZM is $\varepsilon_r=\infty$. Practically, the finite extinction ratio will affect the time-domain intensity distribution of the output optical signal. Therefore, it is crucial to analyze the influence of the finite extinction ratio on the generator performance. As in Fig.4(a), we illustrate the curve of P_Ω/P_{new} when ε_r ranges from 5 dB to 45 dB. It can be seen that when ε_r≥20 dB, the value of P_Ω/P_{new} is almost invariant to 19 dB, which is not affected noticeably by the variation of ε_r. To further verify the effect of ε_r, we introduce a concept of harmonic distortion suppression ratio (*HDSR*), which is defined as the difference of the 1st-order and the maximum interference harmonics. Fig.4(b) shows the curve of *HDSR* versus ε_r varying from 5 dB to 45 dB, and the variation of *HDSR* is roughly kept at 40 dB when ε_r≥20 dB. Accordingly, ε_r larger than 20 dB can satisfy the requirement of our system, and this is easy to implement in the current commercial MZM devices.

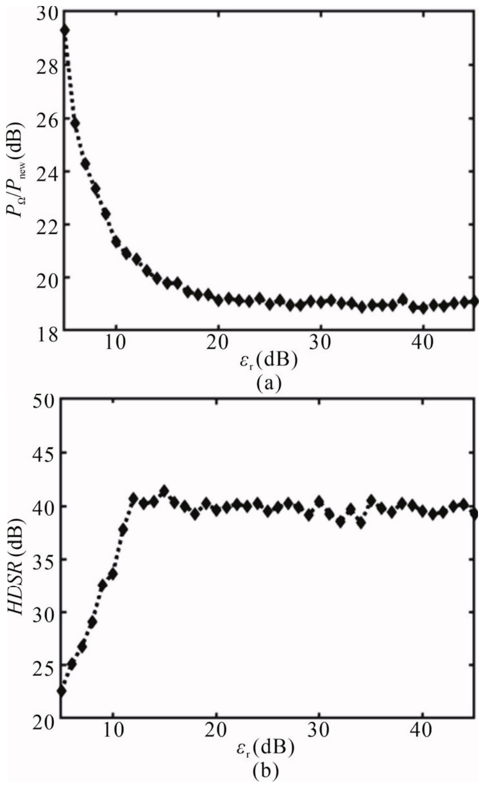

Fig.4 (a) P_Ω/P_{new} versus ε_r; (b) *HDSR* versus ε_r

The Fourier expansion of an ideal rectangular waveform is

$$T_{sq}(t) \propto \cos(\omega t) + \frac{1}{3}\cos(3\omega t) + \frac{1}{5}\cos(5\omega t) + \ldots. \qquad (9)$$

To obtain a rectangular waveform, β_1/β=1/3 is needed according to Fourier expansion in Eq.(9). As $10\lg(\alpha_1^2/\alpha^2)\approx 9.5$ dB, the power ratio of the +1st-order and the newly generated-order sideband P_Ω/P_{new} is around 9.5 dB. The relationship between P_Ω/P_{new} versus G and m are illustrated in Fig.5. In Fig.5(a), setting m=1.05, it is clear that G is approximately 0.306 A when $P_\Omega/P_{new}\approx 9.5$ dB. As for the relationship between P_Ω/P_{new} and m, Fig.5(b) shows that P_Ω/P_{new} is jittering around 9.5 dB when m is within a range from 1 to 1.5, and the oscillation does not exceed 0.42 dB. It also verifies that the rectangular waveform generator's modulation index can be flexibly chosen among values from 1 to 1.5.

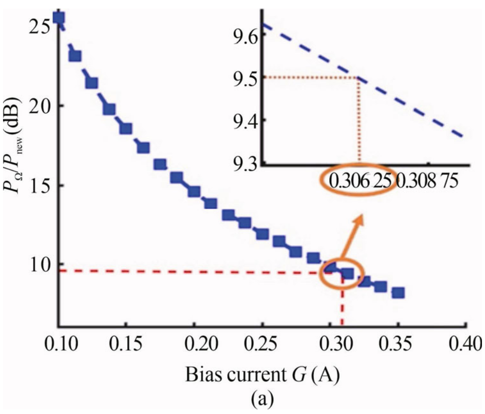

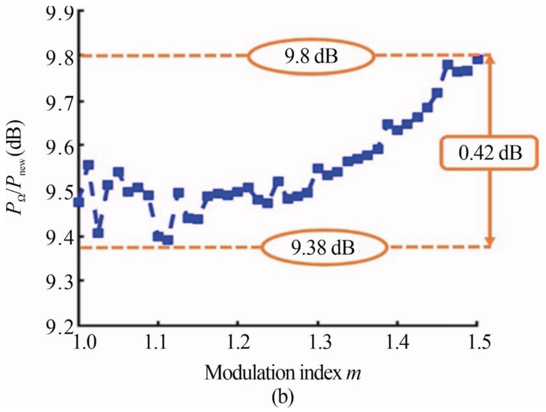

Fig.5 (a) The relevance of P_Ω/P_{new} and the bias current G when m is set as 1.05; (b) The relevance of P_Ω/P_{new} and modulation index m when G is 0.306 A

Our simulation is implemented by the OptiSystem, setting the device parameters in the system in Fig.1 as shown in Tab.1. The frequency of RF signal applied here is 10 GHz. The De-MZM is biased at MITP to carry out the OCS modulation. The optical spectrum, electrical spectrum and temporal waveform of the generated triangular waveform are captured by OSA, ESA and OSC respectively, and the simulation results are shown in Fig.6.

Tab.1 Simulation parameter settings of the triangle waveform generator

Devices	Parameter settings
CW	Central wavelength: 1 550 nm; Power: 10 dBm; Line-width: 0.8 MHz
RF	f_{RF}: 10 GHz
De-MZM	ε_r: 25 dB; Insertion loss: 5 dB; V_π: 4 V; m: 1.43
SOA	G: 0.146 5 A

As the optical spectrum shown in Fig.6(a), the relationship of the 1st-order and the newly generated frequency components is $P_\Omega/P_{new}\approx 19$ dB, which agrees well with the theoretical value stated above. Besides, it also meets the theoretical condition that the power difference between the recovered optical carrier and the 1st-order sideband is large enough. Fig.6(b) shows the electrical spectrum of the triangular waveform which proves that the power difference of 10 GHz to 30 GHz frequency components is roughly 19 dB. Fig.6(c) gives the temporal intensity of the achieved triangular waveform, of which the duty cycle is 1 and the period is 100 ps. For these results, the generation conditions of the triangular waveform are well matched in both frequency domain and time domain. Accordingly, a 10 GHz triangular waveform is successfully generated.

In the previous discussion, the 180° hybrid coupler is with no imbalance. However, there exist unwished phase imbalance in practice. Fig.7 illustrates the impact of 180° hybrid coupler with phase shift within a range from −5% to 5% on P_Ω/P_{new} and *HDSR*, respectively. From Fig.7(a), when the imbalance ratio ranging from −5% to 5%, P_{Ω}/P_{new} is close to 19 dB and remains almost unchanged. Fig.7(b) shows that when the imbalance ratio is within a ±5% range, the values of *HDSR* are all higher than 28 dB, indicating that the interference components are well suppressed. Therefore, the phase imbalance of the 180° hybrid coupler ranging from −5% to 5% is acceptable.

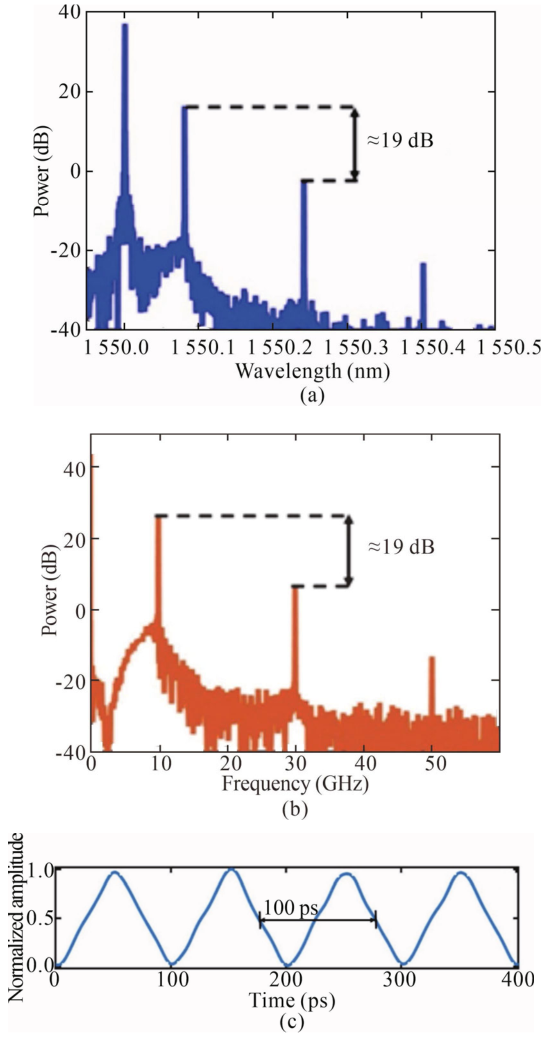

Fig.6 Simulated results of 10 GHz triangular waveform: (a) Optical spectrum; (b) Electrical spectrum; (c) Temporal waveform

In Fig.3(b) mentioned above, when *m* is in range from 1 to 1.5, the values of P_{Ω}/P_{new} are near 19 dB, which is basically inosculate with the desired value for generating the triangular waveform. To intuitively verify the tunable range of *m*, results in Fig.8 simulate the generated triangular waveform when *m* is in and out of this range. Fig.8(a) and (d) show the temporal waveforms and the corresponding electrical spectra in case of *m*=0.63 and *m*=1.83. It can be found that the power difference of 10 GHz to 30 GHz components is greater than 19 dB and the temporal intensity of the waveform is not featured with a triangular shape. When the value of *m* is within this range, for example *m*=1.03 and *m*=1.23 in Fig.8(b) and (c), the power differences are roughly around 19 dB and the obtained temporal waveforms are close to a triangular shape. Accordingly, the desired *m* in our approach is flexible within the range from 1 to 1.5, which is a highlight of our approach.

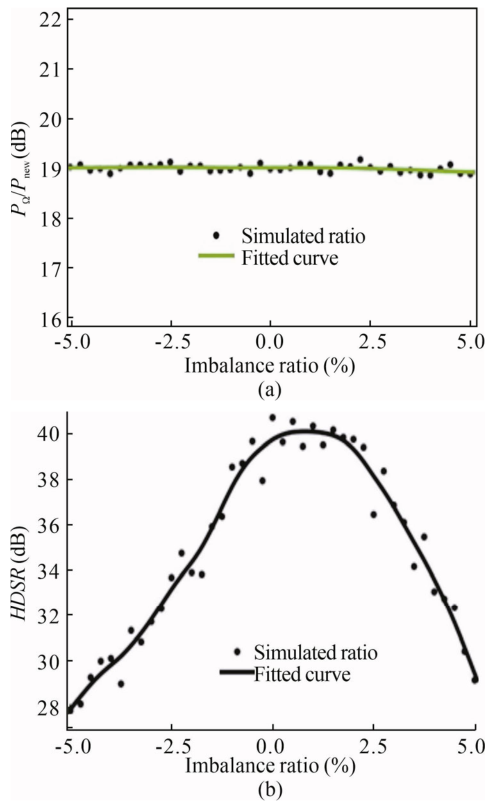

Fig.7 (a) Power ratio P_{Ω}/P_{new} and (b) *HDSR* versus 180° hybrid coupler imbalance ratio ranging from −5% to 5% for the 10 GHz triangular waveform

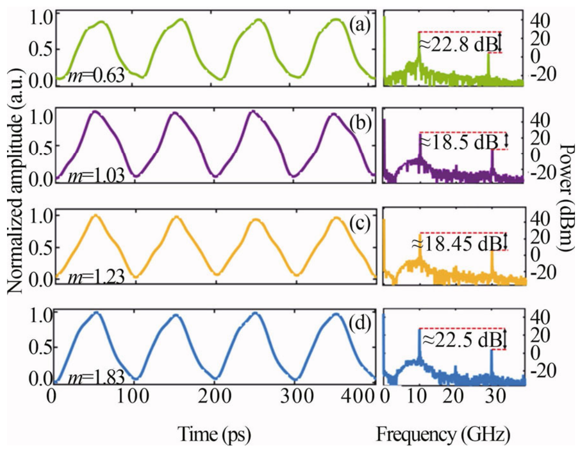

Fig.8 Temporal triangular waveforms and the electrical spectra in case of different *m*

For the rectangular waveform generator, the parameters settings of the devices are basically refer to Tab.1. Differently, the values of *m* and *G* need to be adjusted to 1.05 and 0.306 A, respectively. The optical spectrum, the electrical spectrum and the temporal waveform of the rectangular waveform are observed by OSA, ESA and OSC in Fig.9. As shown in Fig.9(a), the relationship of the 1st-order and the newly generated frequency components is P_{Ω}/P_{new}≈9 dB, which is close to the theoretical value as Eq.(9). The recovered optical carrier is also much higher than other sidebands. In Fig.9(b), the power difference between the 10-GHz and 30-GHz frequency items is 9 dB, and the undesired frequencies are well suppressed. The corresponding temporal waveform is given in Fig.9(c). Therefore, a 10 GHz rectangular waveform with 50% duty cycle is achieved based on our approach.

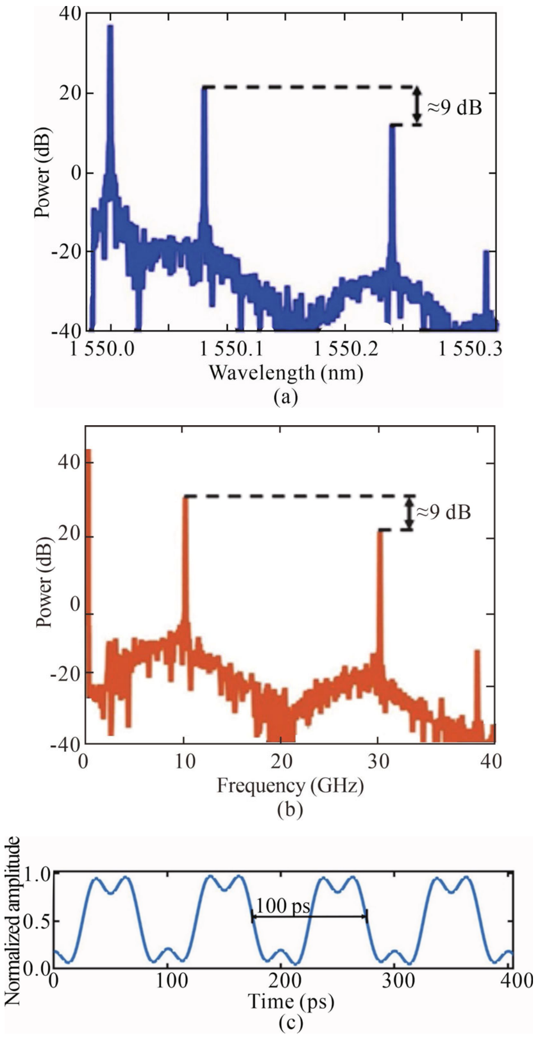

Fig.9 Simulated results of rectangular waveform: (a) Optical spectrum; (b) Electrical spectrum; (c) Temporal waveform

Similar to the work in Fig.7, we discuss the impact of the 180° hybrid coupler imbalance ratio on the rectangular waveform. As in Fig.10(a), the values of P_{Ω}/P_{new} are hardly affected when the imbalance ratio is varying between −5% and +5%. However, the imbalance ratio has a notable influence on the *HDSR* as shown in Fig.10(b), which indicates that the imbalance ratio amplifies the interference component. Supposing that *HDSR* ≥ 24 dB is acceptable, the tolerable range of imbalance ratio is form −1.3% to 5%.

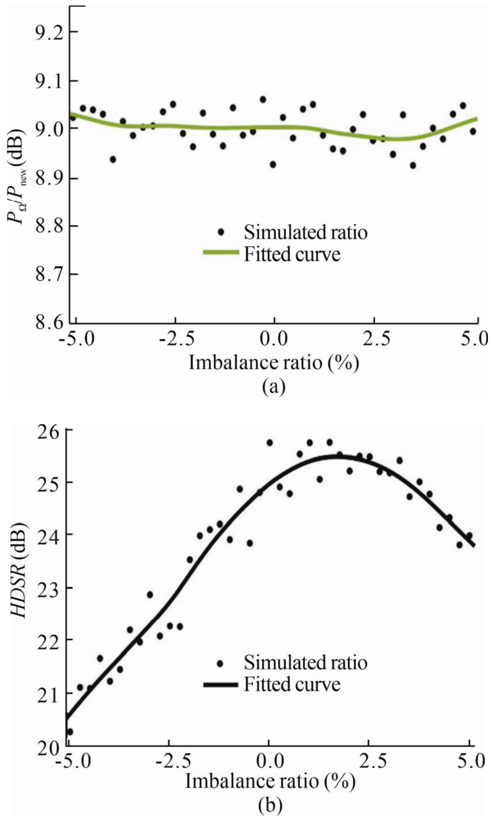

Fig.10 (a) Power ratio P_{Ω}/P_{new} and (b) *HDSR* versus 180° hybrid coupler imbalance ratio ranging from −5% to 5% for the rectangular waveform

As a whole, the scheme put forward is a feasible method to generate triangular and rectangular waveforms. OCS modulation in a De-MZM, FWM in an SOA and optical carrier recover technique are applied to manipulate the spectrum of the generated signal to fit with that of a typical triangular/rectangular waveform. One key highlight is that the desired *m* in OCS modulation is unfixed, which makes the scheme more flexible. To assess the performance of the waveform generator, we discussed the influence of the error caused by the key devices, such as the finite extinction ratio and modulation index drift of the De-MZM, the imbalance ratio of the 180° hybrid coupler. Through analysis, it can be concluded that there exist an acceptable error range to generate target waveforms. Finally, 10 GHz triangular and rectangular waveforms are generated.

Statements and Declarations

The authors declare that there are no conflicts of interest related to this article.

References

[1] WON Y, KIM C, LEE S G. Range resolution improvement of a 24 GHz ISM band pulse radar-a feasibility

study[J]. IEEE sensors journal, 2015, 15(12)：7142-7149.

[2] YAO J P. Photonic generation of microwave arbitrary waveforms[J]. Optics communications, 2011, 284(15)：3723-3736.

[3] KHAN M H, SHEN H, XUAN Y, et al. Ultrabroad bandwidth arbitrary radio frequency waveform generation with a silicon photonic chip-based spectral shaper[J]. Nature photonics, 2010, 4(2)：117-122.

[4] DONG X W, LIU W K, WANG Y P. Dispersion limitation to the waveform synthesis of frequency-to-time-mapping technique[J]. Optik-international journal for light and electron optics, 2019, 187：34-38.

[5] CHI H, WANG C, YAO J. Photonic generation of wideband chirped microwave waveforms[J]. IEEE journal of microwaves, 2021, 1(3)：787-803.

[6] WU T W, ZHANG C F, ZHOU H, et al. Photonic micro-wave waveforms generation based on frequency and time-domain synthesis[J]. IEEE access, 2018, 6：34372-34379.

[7] MA C, YU J, WANG W, et al. Multiple microwave waveform generation by a dual-loop optoelectronic oscillator[J]. Optics communications, 2018, 423：127-133.

[8] ZHANG F Z, GAO B D, PAN S L. Time-domain wave-form synthesis using a dual-polarization modulator[J]. IEEE photonics technology letters, 2016, 28(23)：2689-2692.

[9] JIANG Y, MA C, BAI G F, et al. Photonic microwave waveforms generation based on time-domain processing[J]. Optics express, 2015, 23(15)：19442-19952.

[10] LI X, DU C, LIU F, et al. Photonic generation of microwave arbitrary waveforms using stimulated Brillouin scattering and Sagnac loop[J]. Optoelectronics letters, 2021, 17(6)：379-384.

[11] CHEN Y. Photonic generation and transmission of triangular and square waveforms with a large repetition rate tunable range[J]. Journal of lightwave technology, 2018, 36(16)：3293-3301.

[12] LIU X K, PAN W, ZOU X H, et al. Photonic generation of triangular-shaped microwave pulses using SBS-based optical carrier processing[J]. Journal of lightwave technology, 2014, 32(20)：3797-3802.

[13] LI J, ZHANG X P, HRAIMEL B, et al. Performance analysis of a photonic-assisted periodic triangular-shaped pulses generator[J]. Journal of lightwave technology, 2012, 30(11)：1617-1624.

[14] ZHOU H, SHEN Y, CHEN M, et al. Cost-efficient, polarization-insensitive and widely-tunable AOWC of OFDM signal based on FWM in SOA[J]. Optics express, 2019, 27(26)：38553-38566.

[15] YAN X L. Research of all optical wavelength conversion based on four wave mixing effect[D]. Wuxi：Jiangnan University, 2016：22-29. (in Chinese)